DESIGN IMPROVEMENT OF THE LONGERONS OF A TRAINER AIRCRAFT TOWARDS BETTER CORROSION RESISTANCE

U. Schuster
Pilatus Aircraft Ltd.
Stans, CH-6371
Switzerland

Abstract

The upper and lower Longerons in the Pilatus PC-9(M) principle fuselage structure are made from AA2024-T3511 extruded shapes. This alloy product form is widely used in the aircraft industry, though it has shown poor resistance to exfoliation corrosion in the recent past. The ultimate ambition of this paper is to improve the Longeron corrosion resistance by design. Therefore, general exfoliation corrosion issues and recent advances in aluminium alloys and metallic fuselage design are reviewed. A good design approach is found to be a material supersedure through AA2124-T851 plate in conjunction with integrally machining. To reduce production costs, both upper Longerons are separated into a machined forward and a machined aft section which are connected by a bolted lap-joint. This joint is a major design change and thus invalidates the aircraft fatigue test. In this paper, we perform a joint fatigue analysis using FEM in combination with a strain-life method to predict the minimal crack initiation life and thus allow for FAR-23 certification without structural testing.

1. INTRODUCTION

The Pilatus PC-9(M) is a turboprop trainer aircraft certified under FAR-23 regulations. There are 306 aircraft in service (as per June 2011), including PC-9(M) and the similar products PC-9 and PC-7MkII having an identical main fuselage structure. Figure 1 (appended) shows its conventional aluminium semi-monocoque design with blanked canopy, fuselage skin and engine cowling. As principle structural elements there are two upper and two lower Longerons in the forward fuselage.

Each Longeron is manufactured from an extruded U-section of the WL 3.1354-T3511 aluminium alloy which is essentially equal to AA2024. This legacy alloy is still widely used, though it has shown poor resistance to exfoliation corrosion in the recent past. During maintenance, this type of corrosion was encountered on several Longeron locations of several PC-9(M) aircraft. As Longeron failure is catastrophic design improvements are mandatory to provide increased corrosion resistance.

Therefore, let us briefly review material and design related factors which ultimately initiate and promote corrosion. An introduction to modern aluminium materials and metallic fuselage design enables us to find favourable design improvements. Finally, fatigue analyses must be performed by means of FEM in conjunction with a strain-life approach to allow for FAR-23 certification without structural airframe testing.

2. STATE OF THE ART

2.1. Aluminium Alloys

Over the past decade, the Aging Aircraft Community has invested heavily in research and development for the characterization, prediction, remediation, and prevention of aircraft corrosion. Due to these efforts, which were focused on legacy alloys, corrosion resistance could have been improved dramatically [1]. Apart from advanced legacy alloys, next generation Aluminun-Lithium alloys, like AA2X9X, evolved with superior properties in terms of corrosion resistance, density, stiffness and static strength.

Table 1 summarizes applicable high strength and damage tolerant aluminium alloys and their resistance to exfoliation corrosion (EXCO), considering legacy alloys (AA2024, AA7075) as well as promising advanced legacy alloys (AA2124, AA7475) and Al-Li alloys (AA2099, AA2196). Ratings "A" through "D" indicate the corrosion resistance to EXCO, where "A" means best and "D" means lowest resistance. These values refer to the short transverse direction (ST), as the ST-direction is generally most susceptible and thus governs the total material corrosion performance [2]. Note, that EXCO resistance is also a measure for the material's stress corrosion cracking (SCC) characteristics. Generally, those alloys and tempers that are susceptible to EXCO are also prone to SCC and vice versa [2].

Tab. 1: EXCO ratings for aluminium alloys in ST- direction, [2]

Alloy and Temper	Rolled Plate	Extruded Shapes
AA2024-T3, T4	D	D
AA7075-T6	D	D
AA2124-T8	B	-[1]
AA7475-T73	A	-[1]
AA2099-T83 [2]	-[1]	A
AA2196-T8511 [2]	-[1]	A

[1] product is not yet offered commercially
[2] equivalent rating as per [3]

The advanced legacy alloy AA2124 was primarily developed for elevated temperature applications. It is a higher purity version of AA2024 and essentially provides the same physical properties at higher fracture toughness and improved EXCO resistance [2]. Its primary use is for machined fuselage bulkheads and wing skins in high-performance military aircraft [4]. At Pilatus, this alloy is employed on PC-21 trainer aircraft and is the designated standard material for integrally machined parts [5].
AA7475 is the higher purity version of AA7075 and provides improved corrosion resistance and fracture toughness [6]. In the T73 temper, the plates are artificially over-aged towards best EXCO resistance with a decrease in strength compared to the T6 temper. However, the higher purity increases strength and compensates this effect, so that AA7475-T7 has essentially the same strength as AA7075-T6 [5] but at superior EXCO resistance.

With regard to Al-Li alloys, research and development efforts were made to face the increased utilization of fibre reinforced plastics in large commercial aircraft such as B787 and A350 [7]. Their major performance objectives are strength, fracture toughness, anisotropy, corrosion resistance and fatigue life. As result, the latest Al-Li alloys make metallic options competitive or superior to a composite based design for many aerospace applications [8]. The two most auspicious third generation Al-Li alloys, namely AA2099 and AA2196, shall briefly be introduced.
AA2099-T83 extrusions can already be found in the Airbus A380 fuselage structure [3]. This alloy offers higher strength, lower density, higher stiffness, superior damage tolerance, excellent corrosion resistance, excellent weldability, higher fracture toughness and excellent fatigue crack growth resistance, compared to the incumbent Longeron material AA2024-T3511. These extrusions can replace AA2xxx, AA6xxx, and AA7xxx aluminium alloys in applications such as fuselage structures, lower wing stringers and stiffness-dominated designs [3, 9]. In terms of material allowables Al-Li alloys are generally superior to legacy and advanced alloys [2, 3]. The major disadvantages are the significantly higher costs as well as recycling issues.
AA2196-T8511 extrusion properties are essentially equal to AA2099. They are recommended for parts critical in compression and in damage-tolerant applications as for lower wing stringers [10]. They are employed on the A380 as floor cross beams and fuselage stiffeners [7, 11].

2.2. Metallic Fuselage Design

In terms of aircraft size, configuration, usage and performance, the modern Pilatus PC-21 is similar to the PC-9(M) and thus suitable to highlight recent advances in metallic fuselage design. Figure 2 shows the Longeron arrangement within the aircraft and the Longeron design, exemplary for the lower left hand side. They are integrally machined from AA2124-T8511 plates as one-part upper and three-part lower Longerons, screw-joined at the Frames as shown. The vast majority of the PC-21 structure is made of integrally machined parts, due to evolved integrally machining technology in terms of surface and dimensional quality, cutting speed and possible part size and shape. The integrally machining technology offers considerable aircraft production and operational cost reduction compared to conventional sheet metal design and differential constructions. The key advantages are

- solid procurement due to more trusted availability of plate material compared to extrusions
- plate material promotes stock harmonizing
- machined parts are suitable for outsourcing
- high degree of automation and flexible production
- tailored design and simplified assembly due to less fasteners and components
- automated swarf recycling systems

Roughly spoken, a greater degree of integration offers greater cost savings. To further exploit these advantages of integrally machined parts, so-called integrally stiffened panels (ISP) evolved. An aluminium ISP usually comprises fuselage skin, stiffeners and possibly frames in a single part. A principle production method is called "plate hog-out", where a thick plate is machined to the final shape including skin and stiffeners. Less parts and fasteners reduce assembly time, corrosion traps and also minimize inspection tear-down [12]. ISPs also provide better weight and strength with acceptable Damage Tolerant and Fail Safe behaviour at significantly lower costs [13]. They are easy to maintain but provide limited repairability, dependent upon

stringer(-foot) design. A major technical challenge to ISP structures is damage tolerance and fail safety, such as the arrest of a two-bay crack by integral tear straps [14]. Crack deflection and crack arrest mechanisms are currently being investigated [15] and would require extensive review, if it should come to ISP application for future PC-9(M) fuselages.

3. LONGERON DESIGN

Reference [16] introduces promising structural concepts for improved Longerons. Among the seven considered concepts there are machined split Longerons as well as intergally machined Longerons, heat treatment options, Longeron integration into an ISP and others. The main criteria applied in the concept evaluation scheme claim increased EXCO resistance, low development and manufacturing costs and a production process that provides repeatable Longeron properties as well as the possibility for outsourcing. In this paper, we will focus on the upper Longerons as they are more interesting from a structural standpoint.
In [16] the most favourable design turned out to be a separation of each upper Longeron into a machined forward and a machined aft section which are connected by a bolted lap-joint. Figure 3 shows the joint location between frame (FR) 3D and FR 4. The general Longeron shape remains unchanged, except for thickened lands at the joint to provide for high bearing loads through the fasteners. Figure 4 shows the lap-joint design on the upper left hand Longeron through a virtual skin cutout, looking from outboard. The three segments of the Longeron U-section can be considered as an outboard, top and inboard flange. At the joint, each flange applies two straps. As result, there are three symmetrical double lap joints at each segment of the Longeron U-section. The outboard side additionally comprises the fuselage skin as a strap to avoid inter-rivet buckling due to wide rivet spacing. Further design details are presented in [16].
The strap material is a high strength Titanium alloy Ti-6Al-4V for the inboard and outboard flange straps and SAE4130 HT125 steel for the top flange straps. In conjunction with high strength Hi-Tigue fasteners from Ti-6Al-4V this design allows for a compact joint. For the Longeron material, the alloy AA2124-T851 in the form of plate is chosen as it provides good EXCO resistance, namely "A" in longitudinal (L) and long transverse (LT) direction and "B" through plate thickness (ST). Moreover, this alloy is the designated standard material for machined parts at Pilatus. Longerons from this material promote further stock harmonization and profit by supply guarantee. Subsequent Longeron fatigue analyses require particular material data, namely the Coffin-Manson strain-life curve and the Ramberg-Osgood curve for cyclic stress-strain. These information are currently available for the AA2X24 family, but not for Al-Li alloys. In terms of material costs and recycling issues the chosen material is significantly cheaper than Al-Li. With regard to a direct material supersedure, the A-Basis stress allowables of the new Longeron material AA2124-T851 are throughout superior to WL3.1354-T3511 and AA2024-T3511 [2, 17]. Attention must be given to a slightly lower Young's modulus E. Generally, less Longeron material stiffness would distribute Longeron load into stringers and skin and thus demands an increased Longeron cross section area to compensate for. However, the chemical composition of AA2024, WL3.1354 and AA2124 is basically identical except for the allowed purity [6, 18, 19]. So from a composition point of view, every AA2124 is also an AA2024 and also a WL3.1354. Hence, applying the stiffness provided in [2] would underestimate the Longeron load and probably cause a fatigue problem. So it is conservative to assume AA2024's modulus for the new Longeron material, too. As result, AA2124 provides similar static and fatigue properties and can supersede the incumbent Longeron material AA2024.

4. FATIGUE ANALYSIS

The PC-9(M) primary structure is certified under FAR-23 according to the Safe Life philosophy. The design fatigue life is 10'000 flight hours, corresponding to 20'000 landings, which was verified by a Full Scale Fatigue Test (FSFT). The introduction of the joint is a major design change and thus invalidates the FSFT. In this section we will perform a fatigue life prediction for the upper Longeron joint in order to enable certification without testing. It is most desired not to introduce any inspection cycles but to retain the Safe Life concept and thus minimize direct operating costs for the improved Longerons. Hereinafter, we will consider the left hand joint only, due to symmetry.

4.1. Strain-Life approach

Critical locations for crack initiation on the Longeron joint are the fastener holes. Shear loaded bolted joints are most susceptible to crack initiation and a common source of fatigue failure in aircraft structures [20]. Fastener holes act as a notch and cause high stress concentrations at the root of the notch where local plastic deformation may occur. As long as the surrounding material is still in the elastic range the strain based approach is applicable. Strain-Life refers to low cycle fatigue and is widely used at present [21]. Compared to high cycle fatigue methods, like the Stress-Life approach using S-N curves, the Strain-Life approach is more conservative as the elasto-plastic material behavior is best considered in terms of strain [21, 22].

At Pilatus, the N40 computer program is employed to calculate the crack initiation life from the following input data:

- Material Strain-Life Curve fitted to the Coffin-Manson form
- Material Cyclic Stress-Strain Curve fitted to the Ramberg-Osgood form
- Discrete sequence of maximum principle stress exactly at the root of the notch representing a certain number of cycles

N40 applies a straightforward algorithm. The tracking of the stress sequence accounts for material hysteresis loops and applies the Neuber's Rule, which is an approximate relationship between stress and strain when the material is in the plastic range. The algorithm proceeds with sequence counting of range pairs. The Smith-Watson-Topper equation accounts for the mean stress effect, so that the partial damages of each stress cycle can finally be summed up by the commonly used Miner's Rule and give the crack initiation life. With regard to input data, both material properties are available from in-house tests. What we want to focus on is the derivation of the critical stress sequences, namely at the fastener holes.
The stress at the root of a fastener hole is hereinafter referred to as notch stress. On any fastener hole, the notch stress depends on the combination of the outer joint loads, i.e. Longeron normal load, skin normal load and skin shear. Hence, the notch stress sequence depends on the combination of the individual load sequences. To decrease the degree of freedom and to ease the derivation of the stress sequence it would be advantageous, if the stress could be related to only one single load. Therefore, the above joint loads are required to have a constant ratio. However, any flight manoeuvre comes with a unique ratio of joint loads. Moreover, their individual contribution to notch stress is nontrivial and thus requires a separate analysis for each flight manoeuvre to find the exact sequence of notch stresses. This is not practicable at all and some simplification must be made in order to derive a representative stress sequence from only one master load sequence.
Therefore, our approach is to assume that the majority of flight manoeuvres is symmetrical, i.e. the fuselage is mainly subjected to bending about the aircraft spanwise axis. For all magnitudes of bending moments the ratio of shear and tension loads in the fuselage portion near the joint can be assumed as being nearly constant. Due to this, we can relate each outer joint load to one governing load F_{ref}. As result, the value of F_{ref} does perfectly define the joint load condition. Moreover, as our strain based approach is associated to maximum principle stress, we can assume the stress at each fastener hole to vary with F_{ref} in a linear manner. To establish the linear correlation between the reference load F_{ref} and resulting stresses at each fastener hole, we will developed a local FEM model of the joint.

4.2. Global and local FEM models

Figure 6 shows the considered joint model as a fuselage cutout including the Longeron forward and aft section, joint straps, a split packing between skin and Longeron, the fasteners and a portion of the adjacent skin, which extends to the joint's far-field. All joint members are modelled with least material thickness according to their dimensional tolerances. The simplified Hi-Tigue bolts, nuts and rivets represent a transition fit through zero gap. We use solid parabolic tetrahedral elements (10-noded) throughout as these elements are most suitable to capture high stress gradients in riveted or bolted connections [23]. To model the contact between the fasteners and the joint members, NX NASTRAN offers linear contact properties for solid mesh. Here, "linear" denotes an iterative solution from numerous linear sub solutions. Hence, this method is limited to small displacements and linear material properties. A contact pair, such as bolt shaft and strap hole, comprises two faces which can potentially interact. In the present method, attention is given to similar mesh sizes of contacting faces as this makes results most accurate [24] and not dependent upon a master/slave definition. Moreover, we employ solid elements for the fasteners, which is recommended for bolted structures [23]. Other methods utilize several coaxial line elements as bolt shaft axis and radial line elements extending from the shaft axis to the hole face in several layers, where the element nodes must be matched. To represent the real bolt behavior, the radial line elements must be active in compression and inactive in tension (zero stiffness). This method disables linear analysis and cannot represent bearing stress directly. In our method, element nodes need not be coincident and less modelling time allows for rapid design iterations. Moreover, the solid bolts enable the introduction of bolt preload resulting in pressure underneath the bolt and nut head surface which enables higher accuracy of the fastener hole's near field stress. To further promote the conservative nature of this analysis we define a rather low friction coefficient not to distribute the joint loads through the strap faces but through the bolts.

The yet unknown linear correlation between the reference load F_{ref} and the corresponding notch stresses can be derived from two load conditions, preferably the zero load condition and some reference condition. The latter must be a symmetrical manoeuvre, as discussed above. Therefore we use a +7g steady pitching manoeuvre which is the critical static

load case for the Longeron joint region. Figure 5 shows the global PC-9(M) FEM model and the corresponding airframe deformation (overdone). Freebody (FB) loads are extracted for the highlighted elements marking the joint region. Their introduction into the local joint FEM model provides the maximum values of principle stress σ on each fastener hole at this certain loadcase. Let us define the Longeron normal load (i.e. the sum of all Longeron nodal loads) as governing reference F_{ref}. As result, we can refer the notch stresses to F_{ref} so the yet unknown stress sequence $\sigma(t)$ at each fastener hole depends on the load sequence $F_{ref}(t)$ only.

4.3. Load and stress sequence

With regard to the FSFT some PC-9 aircraft were equipped with several strain gauges recording the strain sequence during representative flight missions. The FSFT did reconstruct these typical flights as recorded. Therefore, the actuator loads were adjusted to match the in-flight aircraft deformation sequence. At Pilatus an FE model of the FSFT was developed. As the load sequences of the actuators are known, they can be introduced into the FE model and as result the sequence of nodal forces on any element can be extracted and thus establish the sequence of the referende load $F_{ref}(t)$. Argument t is discrete and counts data rows consecutively. The sequence comprises approx. 374000 load sets (i.e. values for F_{ref}) representing 1'000 flight hours. In [16] the sequence was adapted to include the critical static load case once. Moreover, reference [16] accounts for fuselage skin buckling. The skin tensile stress in the positive manoeuvres is sufficient to prevent the skin panel, which is adjacent to the joint, from buckling. This is not true for negative manoeuvres. It is conservatively assumed that buckled skin cannot take any normal load so the Longeron must transfer that portion, too. The critical panel buckling load was found in [16] from an analytical criterion accounting for skin normal and shear stresses. A sequence tracking checks each load set. When the skin buckles the reference load $F_{ref}(t)$ additionally comprises the nodal load from the skin. Finally, $F_{ref}(t)$ can be introduced to the N40 program, which filters nonessential values. Remember, that the joint stresses were assumed to linearly vary with the reference load. So the stress sequence at a fastener hole $\sigma(t)$ has essentially the same shape as $F_{ref}(t)$. Moreover, $\sigma(t)$ must have its maximum σ_{max} at the critical load case. The stress sequence $\sigma(t)$ can be normalized to this maximum value. This normalized sequence is counted by N40, which applies a range pair counting technique [21].

4.4. Results

To afford certification without testing we consider a conservative scatter factor $SF = 8$. So the minimum required Longeron joint life is

$$L_{CI,req} = SF \cdot 10'000 \text{ h} = 80'000 \text{ h} \quad (1)$$

where L_{CI} denotes the crack initiation life. Based on the normalized stress sequence, L_{CI} can be plotted against any maximum sequence stress σ_{max}. Figure 7 does that for all Longeron joint member materials. The maximum values occur at the critical static load case which are known from the above developed FEM model. Finally, tab.2 presents the reserve factor

$$RF = \frac{L_{CI}}{L_{CI,req}} \quad (2)$$

for each Longeron joint member. As result all joint members provide the required crack initiation life. The least reserve factor $RF_{min} = 1{,}67$ can be found at the skin's foremost Hi-Tigue fastener hole. This value can hardly be validated. However, reference [16] employs the FALLSTAFF sequence as a reference, even though it is only applicable to the wing root of fighter aircraft. At the same skin hole the reserve factor under FALLSTAFF conditions is $RF_{min,Fallstaff} = 2{,}06$.
So the joint structural integrity is additionally demonstrated under FALLSTAFF loading. Finally, the fatigue performance of the the new Longeron material can be compared to the incumbent material to validate the direct material supersedure. In fig.7 the incumbent material AA2024-T3 is not included, but the fatigue performance essentially equals AA2024-T42. On the basis of the derived Longeron joint load sequence, one can say, that in the region of typical aircraft lives the new Longeron material is well superior and can directly supersede the incumbent. As result, the presented static and fatigue analysis can finally verify the structural integrity of the new Longerons.

4.5. Design Review

In a last step the final Longeron design shall be reviewed in terms of structural efficiency and other possible solutions. With regard to joint static and fatigue reserve factors the skin is most critical. The stress at a fastener hole is a combination of bypass load (from skin shear and normal load) and the bearing load from the fastener. As the skin is highly stressed in the critical load case, it must not be further stressed as a joint member. Therefore, different strap materials and thicknesses can adjust the joint stiffness and unload the skin, i.e. the fasteners do not introduce any bearing load into the skin. Figure 8 shows the longitudinal skin stress for several joint strap materials. From (a) through (c) the strap stiffness increases. At

the joint, this increasingly takes tensile load from the skin. In case (c) the joint is too stiff and again introduces bearing loads through the fasteners. Case (d) represents the final joint design which was found after several iterations varying materials, thicknesses and fastener arrangement. In this configuration the skin bearing loads from the Hi-Tigue fasteners are negligible, i.e. the notch stress is exclusively due to bypass load.

5. SUMMARY

Exfoliation corrosion was found on Pilatus PC-9(M) Longerons. The initial problem is poor corrosion resistance of AA2024-T3 in the form of extruded shapes. Substantial progress in the development of modern aluminium alloys offered promising candidates for improved Longerons. As machning technology evolved the most efficient concept was found to be machined Longerons made from an advanced legacy alloy, namely AA2124-T851 plates. Therefore, the Longerons were split into a forward and an aft section, both connected by a bolted lap-joint. The introduced joint raised a major structural issue. In order to enable Longeron certification without testing, thorough fatigue analyses were performed. The critical locations are the fastener holes, where local yielding may occur. Thus, a strain-life approach was applied. To find the crack initiation life, a stress sequence was developed based on the FSFT FE model that also accounts for joint loads due to skin buckling. Finally, structural integrity of the Longeron joint was demonstrated for the developed sequence as well as for the FALLSTAFF sequence. All structural analyses were performed conservatively throughout and the rather high reserve factors do not require structural testing for certification so that development costs can be kept at a minimum. To address exfoliation corrosion as an increasingly important issue on ageing airframes comprising extruded legacy alloys, it was shown that the new Longeron material AA2124 is suitable to directly supersede the incumbent AA2024 as it provides superior static and fatigue performance as well as corrosion resistance. As result, the presented Longerons do well satisfy the ultimate ambition of this work. Their utilization for future PC-9, PC-7MkII and PC-9(M) aircraft can be recommended without reservation.

References

[1] J.P. Moran, R.J. Rioja, and E.L. Colvin. *Improvements in Corrosion Resistance offered by Newer Generation Aluminum Alloys for Aerospace Applications*, 2007. Proceedings of the Light Metals Technology Conference.

[2] US Department of Defense. *Metallic Materials and Elements for Aerospace Vehicle Structures*, mil-hdbk-5h edition, 1998.

[3] C. Giummarra, B. Thomas, and R.J. Rioja. *New Aluminum Lithium Alloys for Aerospace Applications*. Alcoa Lafayette Works and Alcoa Technical Center, 2007.

[4] Alcoa Inc. *Web Catalogue: AA2124 Aluminum Alloy Plate*. `http://www.alcoa.com/global/en/products/product.asp?prod_id=597&Product=&Category=&Query=2124&page=0`, [08-June-2011].

[5] Pilatus Aircraft Ltd. *Aluminium*, 2003. Engineering Standard ES3601.

[6] E. Simmchen. *Luft- und Raumfahrtwerkstoffe*. Dresden University of Technology, 2007. Lecture Notes.

[7] K.H. Rendigs and M. Knüwer, editors. *Metal Materials in Airbus A380*. Izmir Global Aerospace & Offsett Conference, 2010.

[8] J. Hirsch, B. Skrotzki, and G. Gottstein. *Aluminium Alloys: Their Physical and Mechanical Properties*, volume 1. Wiley-VCH, 2008.

[9] Alcoa Inc. *Web Catalogue: AA2099 Aluminum Alloy Plate*. `http://www.alcoa.com/global/en/products/product.asp?prod_id=1827`, [09-June-2011].

[10] Alcan Aerospace. *2196-T8511 Al-Li Extrusions*, 2007. Technical Data Sheet.

[11] Ph. Lequeu, Ph. Lassince, and T. Warner. Aluminum Alloy Development for the Airbus A380. *Advanced Materials and Processes*, 2007.

[12] ASM AeroMat Conference 2006. *Aerospace Alloys Advance At Alcoa*, 2006.

[13] R.G. Pettit, J.J. Wang, and C. Toh. *Validated Feasibility Study of Integrally Stiffened Metallic Fuselage Panels for Reducing Manufacturing Costs*, 2000. NASA Contractor Report 2000-209342.

[14] J. Munroe, K. Wilkins, and M. Gruber. *Integral Airframe Structures — Validated Feasibility Study of Integrally Stiffened Metallic Fuselage Panels for Reducing Manufacturing Costs*, 2000. NASA Contractor Report 2000-209337.

[15] L.L. Prieto. *Modelling and Analysis of Crack Turning on Aeronautical Structures*. PhD thesis, Universitat Politecnica De Catalunya, 2007.

[16] U. Schuster. *Design Improvement of the Upper and Lower Longerons of a Training Aircraft Towards Better Corrosion Resistance*. Pilatus Aircraft Ltd., 2011. Diplomarbeit, Technische Universität Dresden.

[17] Werkstoff Leistungsblätter. *WL3.1354 Aluminium- Knellegierung mit etwa 4,5 Cu -1,5 Mg - 0,6 Mn, Beiblatt 1*, 1983.

[18] SAE International. *SAE AMS4101 - Aluminum Alloy, Plate 4.4Cu - 1.5Mg - 0.60Mn (2124-T851)*, 1978. Aerospace Material Specification.

[19] SAE International. *SAE AMS-QQ-A-200/3: Aluminum Alloy 2024, Bar, Rod, Shapes, Tube and Wire, Extruded*, 1997. Aerospace Material Specification.

[20] H. Huth. *Zum Einfluss der Nachgiebigkeit mehrreihiger Nietverbindungen auf die Lastuebertragungs- und Lebensdauervorhersage*. Fraunhofer-Institut fuer Betriebsfestigkeit (LBF), Darmstadt, 1984.

[21] D. Quaranta. *N40 Crack Initiation - User's Guide*, 2011.

[22] J. Schijve. *Fatigue of Structures and Materials*. Springer, 2009.

[23] T. Stehlin. *Fatigue Analysis of Riveted or Bolted Connections Using the Finite Element Method*, 2003.

[24] EnDuraSim Pty Ltd. *Contact Modelling in Femap with NX Nastran*, 2009.

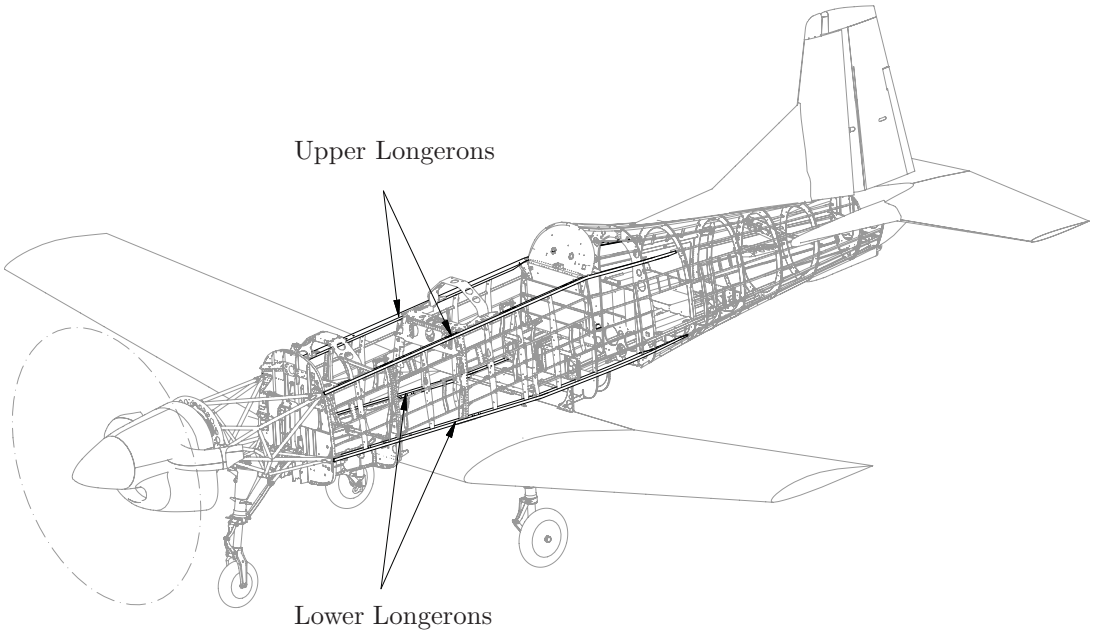

Fig. 1: The four Longerons within the PC-9(M) structure

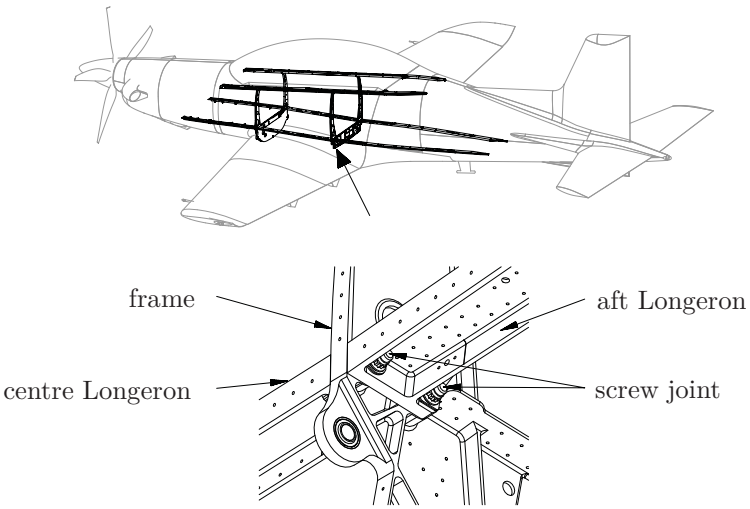

Fig. 2: PC-21 lower left hand Longeron, screw joint

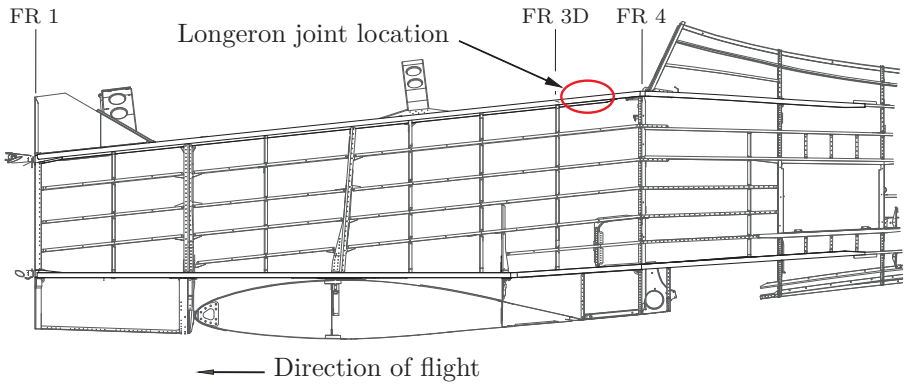

Fig. 3: PC-9(M) forward fuselage and Longeron joint location

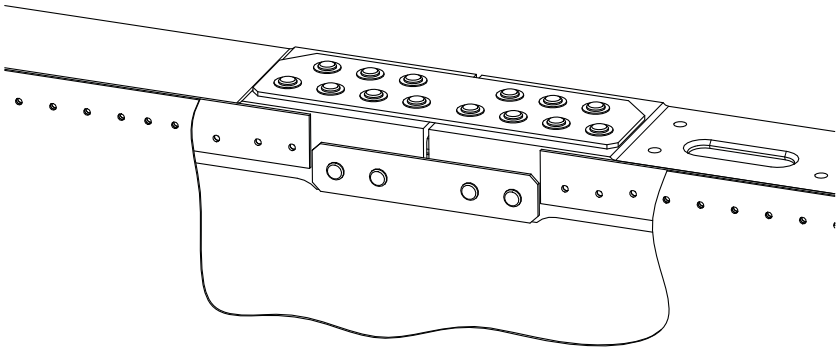

Fig. 4: Longeron lap-joint design

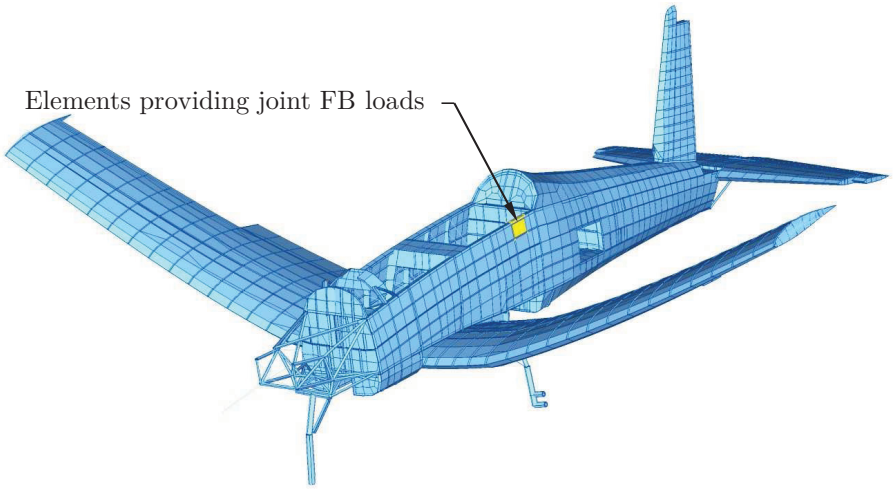

Fig. 5: PC-9(M) FEM model without canopy at the critical load case (displacements x10).

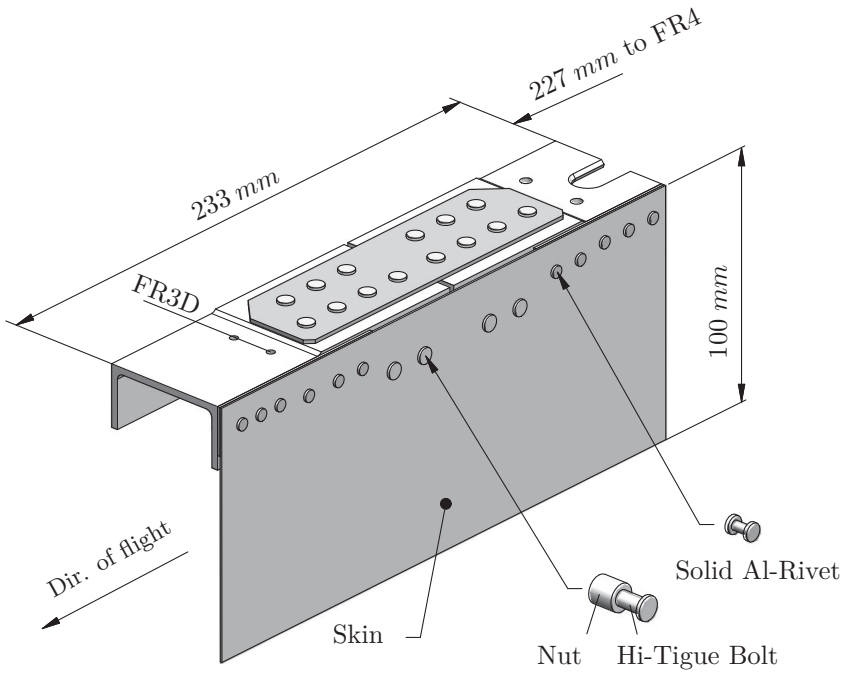

Fig. 6: Longeron joint FEM model

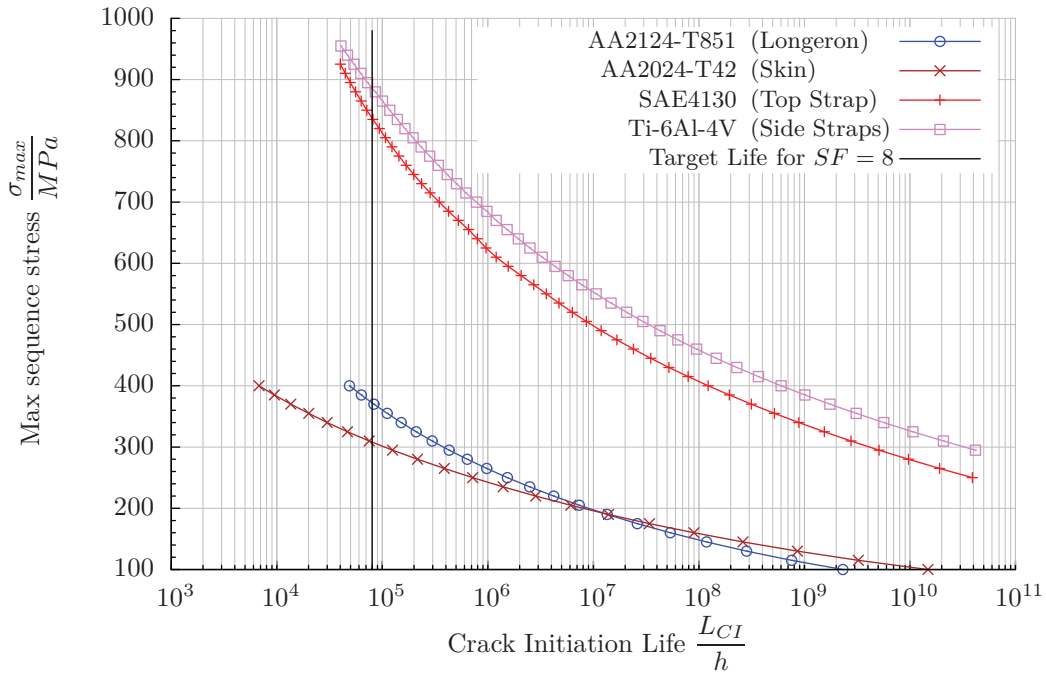

Fig. 7: Max sequence stress and crack initiation life

Tab. 2: Fatigue life results

Joint Member	**Longeron**	**Steel Straps**	**Ti Straps Hi-Tigue bolts**	**Skin**
Material	AA2124-T851	SAE4130-HT125	Ti-6Al-4V	AA2024-T42
$\sigma_{max,seq}$ [MPa]	293	571	415	293
L_{CI} [h]	$4{,}51 \cdot 10^5$	$2{,}43 \cdot 10^6$	$3{,}66 \cdot 10^6$	$1{,}34 \cdot 10^5$
min. RF [-]	5,63	30,3	45,7	1,67

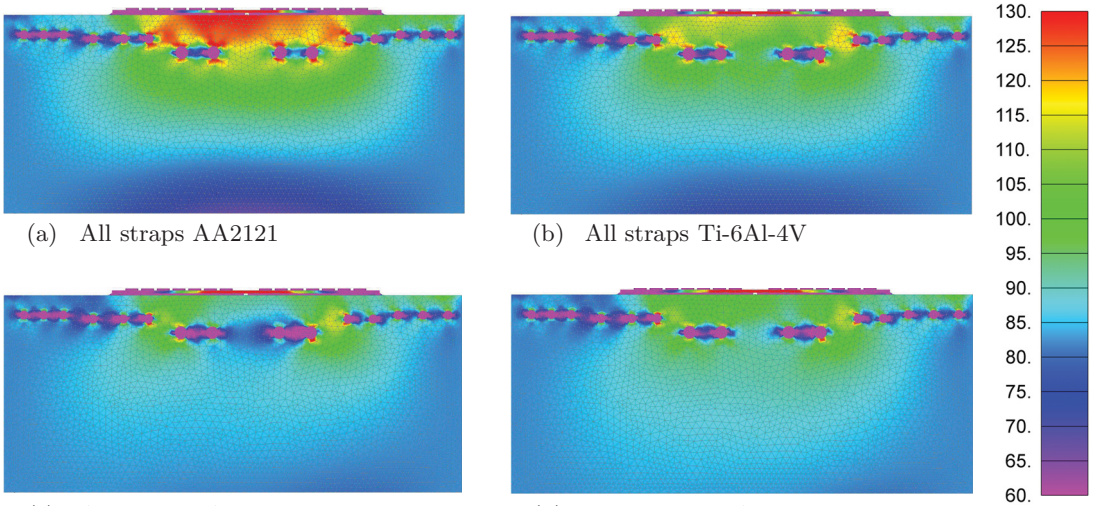

(a) All straps AA2121

(b) All straps Ti-6Al-4V

(c) All straps SAE4130

(d) Top Straps: SAE4130
Side Straps: Ti-6Al-4V

Fig. 8: Skin longitudinal stress in MPa for different strap materials